2021 60th IEEE Conference on Decision and Control (CDC)
December 13-15, 2021. Austin, Texas

Natural Deadlock Resolution for Multi-agent Multi-Swarm Navigation

Boyang Zhang[1] and Henri P. Gavin[1]

2021 60th IEEE Conference on Decision and Control (CDC) | 978-1-6654-3659-5/21/$31.00 ©2021 IEEE | DOI: 10.1109/CDC45484.2021.9683102

Abstract— **This paper presents a nonlinear and discontinuous control scheme for two-dimensional (2-D) multi-agent multi-swarm navigation that resolves deadlocks, without heuristics, by agents reacting purely to their constrained dynamics. The method is based on extensions of Gauss's Principle of Least Constraint that dynamically identify, incorporate, and stabilize time-varying sets of constraints and that integrate actuator saturation and delay. The deadlocks are naturally resolved by formulating the 2-D leader following and collision avoidance requirements as decomposed inequality constraints along the X and Y axes and by asymmetrically assigning zero collision avoidance constraint value to a specific branch. Numerical results are presented for two agents and two 15-agent swarms resolving nominal deadlocks at a computation time order of 10 microseconds, demonstrating the efficacy and efficiency of the proposed approach.**

I. Introduction

Multi-agent swarms are gaining more attention in diverse applications such as exploration, surveillance, and rescue [1]. One remaining challenge for controlling multi-agent swarms is the avoidance of inter-agent collision and the resolution of deadlocks [2]. Deadlocks can occur when some or all agents in multi-agent swarms are involved in inter-agent collisions that result in the system stagnating instead of navigating to its goal. Existing methods of handling collision avoidance for multi-agent navigation include velocity obstacles (VO) [3], [4], artificial potential fields (APF) [5], [6], mixed-integer programs (MIP) [7], [8], and control barrier functions (CBF) [9], [10]. Having merits in their own, each of these methods may have shortcomings under certain scenarios. For examples, VO methods [3], [4] assume constant speeds in crash avoidance and do not guarantee the solution uniqueness. APF methods [5], [6] assume infinite control actions for collision avoidance close to agents' surfaces, and the solution could be trapped into local minima. MIP [7], [8] become computationally expensive when the swarm size becomes large, while CBF approaches [9], [10] do not incorporate actuation delay and may not be computationally cheap when the goal positions do not remain stationary in solving the constrained optimization problem. Furthermore, not all of these approaches have a deadlock resolution, and they are not in general guaranteed to pursue the goal within a given time span.

In the navigation of large scale two-dimensional (2-D) multi-agent systems, the coordinated motion for multiple agents as a unit is more important than the planned trajectory of each individual agent to perform cooperative tasks [1]. In this paper, we propose a control framework for multi-agent multi-swarm (MAMS) navigation with collision avoidance, deadlock resolution, goal pursuit within a specific time frame, and actuator saturation and delay. Our approach is based on the extended Gauss's Principle of Least Constraint (GPLC) [11].

The original GPLC, along with its mathematically equivalent counterpart, the Udwadia-Kalaba (U-K) equations [12], has been applied to control multi-agent systems of small numbers [13], [14]. However, neither the original GPLC nor the U-K equations can accommodate inequality constraints, actuator saturation, or actuator delay.

This paper extends our previous work on GPLC control scheme that demonstrated collision free navigation of a dense swarm of hundreds of agents [11]. Neither deadlock resolution nor multi-swarm control was addressed in this initial study. In [11], leader following and collision avoidance constraints are scalar constraints on relative distances.

This paper starts with a Lagrangian perspective to derive the GPLC Karush-Kuhn-Tucker (KKT) system. Constraints are formulated for X and Y coordinates in a componentwise manner, and deadlock resolution is naturally achieved by selecting the set of bounds which may be satisfied by strict inequalities and the set that are satisfied with equality or inequalities.

Fundamentally, the approach developed herein allows for constraint violation, by design, in order to compute control actions that adaptively negotiate agents' trajectories into admissible configurations. The set of active inequality constraints changes dynamically and is identified without iterations. The KKT formulation of the GPLC allows for the incorporation of actuator saturation and delay and distinguishes control forces due to different constraints. Moreover, the method naturally resolves deadlock configurations, without the need for case-dependent heuristics. The equations of motion of the closed-loop system are unique, and the method is computationally efficient.

In the following, we present a new derivation of the GPLC in Section II and formulate 2-D MAMS navigation problem in Section III. Next, numerical studies on agent-agent and swarm-swarm head-on collision are presented in Section IV, followed by the conclusions and future work in Section V.

II. Preliminaries for Constrained Dynamics

A. Gauss's Principle of Least Constraint (GPLC)

GPLC provides a perspective on the effect of constraints on the motion of mechanical systems described by generalized coordinates $\mathbf{q}(t) \in \mathbb{R}^{2N}$, having symmetric positive

This work was supported in part by the U.S. Army Research Office under award number 75568-NS-II.

[1]B. Zhang and [1]H.P. Gavin are with Department of Civil and Environmental Engineering, Duke University, Durham, NC, 27708 USA boyang.zhang@duke.edu, henri.gavin@duke.edu.

definite mass matrices $\mathbf{M} \in \mathbb{R}^{2N \times 2N}$ and subject to C active constraints

$$\mathbf{g}(\mathbf{q}, t) = \mathbf{c} \tag{1}$$

at any time instant, where $\mathbf{c}$ denotes constant thresholds. The GPLC framework requires that the constraint functions, $\mathbf{g} : \mathbb{R}^{2N+1} \to \mathbb{R}^C$, be at least twice differentiable in time such that

$$\frac{d^2}{dt^2}\mathbf{g}(\mathbf{q}, t) = \frac{\partial \mathbf{g}}{\partial \mathbf{q}}\ddot{\mathbf{q}} + \frac{d}{dt}\left(\frac{\partial \mathbf{g}}{\partial \mathbf{q}}\right)\dot{\mathbf{q}} + \frac{\partial^2 \mathbf{g}}{\partial t^2} = \mathbf{0} \tag{2}$$

are linear in the coordinate accelerations, $\ddot{\mathbf{q}}$. Equation (2) may be compactly written as

$$\mathbf{A}(\mathbf{q}, t)\, \ddot{\mathbf{q}} = \mathbf{b}(\mathbf{q}, \dot{\mathbf{q}}, t)\ , \tag{3}$$

where

$$\mathbf{A}(\mathbf{q}, t) = \frac{\partial \mathbf{g}}{\partial \mathbf{q}} = \begin{bmatrix} \frac{\partial g_1(\mathbf{q},t)}{\partial q_1} & \cdots & \frac{\partial g_1(\mathbf{q},t)}{\partial q_{2N}} \\ \vdots & \ddots & \vdots \\ \frac{\partial g_C(\mathbf{q},t)}{\partial q_1} & \cdots & \frac{\partial g_C(\mathbf{q},t)}{\partial q_{2N}} \end{bmatrix} . \tag{4}$$

The Lagrangian for the dynamical system can be defined as

$$L = T - V \tag{5}$$

where $T = \dot{\mathbf{q}}^{\mathsf{T}}\mathbf{M}\dot{\mathbf{q}}/2$ denotes the kinetic energy, and V denotes the potential energy depending only on $\mathbf{q}$.

Noting that $\mathbf{g} - \mathbf{c} = \mathbf{0}$ for any time t, the Lagrangian L may be adjoined with $-\boldsymbol{\lambda}^{\mathsf{T}}(\mathbf{g} - \mathbf{c})$ such that

$$\bar{L} = L - \boldsymbol{\lambda}^{\mathsf{T}}(\mathbf{g} - \mathbf{c})\ , \tag{6}$$

where $\boldsymbol{\lambda} \in \mathbb{R}^C$ contains the Lagrange multipliers associated with the active constraints (1).

Applying Euler-Lagrange differential equations to the augmented Lagrangian $\bar{L}$, we obtain the constrained equations of motion

$$\begin{aligned} & \frac{d}{dt}\left(\frac{\partial \bar{L}}{\partial \dot{\mathbf{q}}}\right) - \frac{\partial \bar{L}}{\partial \mathbf{q}} = \mathbf{0} \\ \Longrightarrow \quad & \frac{d}{dt}\left(\frac{\partial T}{\partial \dot{\mathbf{q}}}\right) + \frac{\partial V}{\partial \mathbf{q}} + \boldsymbol{\lambda}^{\mathsf{T}}\frac{\partial \mathbf{g}}{\partial \mathbf{q}} = \mathbf{0} \\ \Longrightarrow \quad & \mathbf{M}\ddot{\mathbf{q}} - \mathbf{f}(\mathbf{q}) + \mathbf{A}^{\mathsf{T}}\boldsymbol{\lambda} = \mathbf{0}\ , \end{aligned} \tag{7}$$

where $\mathbf{f}(\mathbf{q}) = -(\frac{\partial V}{\partial \mathbf{q}})^{\mathsf{T}}$ are the nonconstraint forces due to a conservative potential V.

Combining $2N$ equations (7) with C double-differentiated constraint equations (3), we obtain $2N + C$ equations

$$\begin{bmatrix} \mathbf{M} & \mathbf{A}^{\mathsf{T}} \\ \mathbf{A} & \mathbf{0} \end{bmatrix} \begin{bmatrix} \ddot{\mathbf{q}} \\ \boldsymbol{\lambda} \end{bmatrix} = \begin{bmatrix} \mathbf{f} \\ \mathbf{b} \end{bmatrix} \tag{8}$$

linear in $2N + C$ unknowns, where $\mathbf{0}$ denotes a zero matrix. $\mathbf{f}_{\mathrm{c}} \triangleq -\mathbf{A}^{\mathsf{T}}\boldsymbol{\lambda}$ represents the actions required to enforce the constraints. The GPLC KKT system (8) is equivalent to that in [11] which is derived from a Newtonian perspective.

The controlled space for the system is defined based on the equality constraints $\mathbf{g}_{\mathrm{eq}} = \mathbf{c}_{\mathrm{eq}}$ and the inequality constraints $\mathbf{g}_{\mathrm{in}} \leq \mathbf{c}_{\mathrm{in}}$. At each time instant, the active constraint set is identified as the collection of all equality constraints and all inequality constraints that exceed their corresponding thresholds. This set of C active constraints is treated as equality constraints $\mathbf{g} = \mathbf{c}$ and varies over time according to the natural evolution of constrained system dynamics.

In the navigation of individual agents within MAMS systems via GPLC, the feedback control law results from a set of holonomic constraints that describes the desirable behaviors of those agents (i.e., a subswarm): to keep each agent close enough to its virtual leader and far enough away from their neighbors. The constraint forces $\mathbf{f}_{\mathrm{c}}$ computed via the GPLC approach can be interpreted as the control actions required to move agents to admissible trajectories. These control actions are saturated and delayed in order to model realistic limitations on actuator capacity and bandwidth. The resulting control scheme is nonlinear and discontinuous.

B. Existence and Uniqueness of the solution of KKT Systems

Proposition 1: The MAMS systems considered in this study has a diagonal positive definite mass matrix, thus (8) is singular if and only if $\mathbf{A}^{\mathsf{T}}$ has a nontrivial null space.

Proof: See Proposition 1 in [11]. ■

C. Stabilization of Active Constraints

Enforcing (3) does not necessarily satisfy (1) due to numerical errors which can accumulate in explicit finite-precision numerical integration. Furthermore, the unavoidable realistic issues of exogenous disturbance, actuator saturation and delay, and inconsistent initialization (i.e., initial states that violate constraints) may drive the coordinate trajectories to deviate from one or more constraint. In control via GPLC, the command control actions result from active constraints, and the constraint errors are asymptotically stabilized by Baumgarte's stabilization [15] so that $\ddot{g} = 0$ is replaced with

$$\ddot{g} + 2\zeta\omega\dot{g} + \omega^2(g - c) = 0\ , \tag{9}$$

where g is any linearly independent element (due to Proposition 1 to guarantee the existence and uniqueness of the solution) of the vector of active constraints $\mathbf{g}$. Applying (9) to the set of active constraints $\mathbf{g}$ at each time step (with possibly different values for ω and ζ in each constraint) and representing them in a more compact manner, we obtain

$$\mathbf{A}(\mathbf{q}, t)\, \ddot{\mathbf{q}} = \widehat{\mathbf{b}}(\mathbf{q}, \dot{\mathbf{q}}, t)\ , \tag{10}$$

where $\widehat{\mathbf{b}}$ now contains terms involving ω and ζ. Compared to $\mathbf{b}$ in (3), ω and ζ may be respectively regarded as the natural frequency and damping ratio of the *constraint oscillators* and therefore may be viewed as adjustable control parameters.

Combining (7) with the stabilized constraints (10) yields

$$\begin{bmatrix} \mathbf{M} & \mathbf{A}^{\mathsf{T}} \\ \mathbf{A} & \mathbf{0} \end{bmatrix} \begin{bmatrix} \ddot{\mathbf{q}} \\ \boldsymbol{\lambda} \end{bmatrix} = \begin{bmatrix} \mathbf{f} \\ \widehat{\mathbf{b}} \end{bmatrix}\ , \tag{11}$$

which we term the GPLC KKT system with constraint stabilization.

D. Regularization

In the navigation of large scale MAMS systems, $\mathbf{A}$ may be a tall matrix, i.e., $C > 2N$. In addition, some active constraints may not be linearly independent at some time instants. In this study, we regularize the system (11) as [11]

$$\begin{bmatrix} \mathbf{M} & \mathbf{A}^{\intercal} \\ \mathbf{A} & -\beta\mathbf{I} \end{bmatrix} \begin{bmatrix} \ddot{\mathbf{q}} \\ \boldsymbol{\lambda} \end{bmatrix} = \begin{bmatrix} \mathbf{f} \\ \widehat{\mathbf{b}} \end{bmatrix} \ , \tag{12}$$

where $\mathbf{I}$ denotes an identity matrix, $0 < \beta \ll m$ is the regularization factor, and the original problem (11) is attained for $\beta = 0$. The solution of (12) is a unique approximate solution of (11).

III. Swarm of Swarms Navigation

Our problem at hand is a swarm of K swarms navigating in a Cartesian plane. Each subswarm is assigned a guiding virtual leader with position coordinates $\bar{\mathbf{p}}_k(t) = [\bar{x}_k(t)\ \bar{y}_k(t)]^{\intercal} \in \mathbb{R}^2$ and has a number of N_k agents, $k = 1, \ldots, K$ such that $\sum_{k=1}^{K} N_k = N$. Agent i has a constant mass m_i and is at the position coordinates $\mathbf{p}_i(t) = [x_i(t)\ y_i(t)]^{\intercal} \in \mathbb{R}^2$, $i = 1, \ldots, N$. Note that the standard multi-agent point-to-point navigation problem in which each agent has its own goal position can be attained by setting $K = N$ and $N_k = 1$, $\forall k$, and by prescribing each agent's virtual leader stationary at the agent's goal. Thus, our problem formulation is more general than the standard multi-agent point-to-point navigation.

In the following, the sub/superscripts u, l, x, and y denote upper bound, lower bound, X component, and Y component, respectively. The subscript k refers to the index of the subswarm and thus the virtual leader, while the subscripts i and j denote the indices of agents. The sub/superscripts are used where appropriate to denote the relevant physical quantities.

A. Unconstrained Dynamics

We assume that each agent i within the MAMS system is subjected to double integrator dynamics,

$$\begin{bmatrix} m_i & 0 \\ 0 & m_i \end{bmatrix} \begin{bmatrix} \ddot{x}_i \\ \ddot{y}_i \end{bmatrix} = \begin{bmatrix} f_i^{\mathrm{x}} \\ f_i^{\mathrm{y}} \end{bmatrix} \ , \tag{13}$$

where f_i^{x} and f_i^{y} are respectively the nonconstraint forces exerted on agent i along the X and Y axes and could result from environmental or adversarial processes.

B. Constraints

Let subswarm $k \in \{1, \ldots, K\}$ be constrained to follow its virtual leader at $\bar{\mathbf{p}}_k(t)$. We want all agents in the subswarm to follow their virtual leader within a rectangle centered at $\bar{\mathbf{p}}_k$ with edge lengths $2\mathbf{d}_k = 2[d_k^{\mathrm{x}}\ d_k^{\mathrm{y}}]^{\intercal} \in \mathbb{R}^2$. Mathematically, the leader following constraints are

$$\mathbf{g}_{ik} = [g_{ik}^{\mathrm{x}}\ g_{ik}^{\mathrm{y}}]^{\intercal} \triangleq |\Delta\mathbf{p}_{ik}| = |\mathbf{p}_i - \bar{\mathbf{p}}_k| \leq \mathbf{d}_k \ , \tag{14}$$

where $|\cdot|$ denotes absolute value, and the inequality sign denotes componentwise comparison.

Pairwise collision must be avoided for all adjacent agent pairs $\{i, j\}$. We enclose each agent within a virtual rectangular buffer so that for agent pair $\{i, j\}$ the buffer size between them along the X and Y axes are $\mathbf{r}_{ij} = \mathbf{r}_{ji} = \mathbf{r}_i + \mathbf{r}_j = [r_{ij}^{\mathrm{x}}\ r_{ij}^{\mathrm{y}}]^{\intercal} \in \mathbb{R}^2$. Mathematically, the collision avoidance constraints are

$$\mathbf{g}_{ij} = [g_{ij}^{\mathrm{x}}\ g_{ij}^{\mathrm{y}}]^{\intercal} \triangleq |\Delta\mathbf{p}_{ij}| = |\mathbf{p}_i - \mathbf{p}_j| \geq \mathbf{r}_{ij} \ . \tag{15}$$

Note that only the ordered pair $\{i, j\}$, rather than both $\{i, j\}$ and $\{j, i\}$, is considered to avoid repeating constraints.

Constraints (14) are convex while (15) are nonconvex. Note that the constants $\mathbf{d}_k$ and $\mathbf{r}_{ij}$ can assume different values if the swarm of swarms at hand is heterogeneous.

C. Constraint Error Stabilization

During the natural evolution of the constrained MAMS dynamics, the active inequality constraints (14) and (15) are dynamically determined by comparing the involved relative distances to their corresponding thresholds. The active constraints are then double differentiated as (2), stabilized as (10), and incorporated into the system (12) at each time step.

Agent i is not following its leader closely enough if $\mathbf{g}_{ik}$ is active along at least one dimension, while the agent pair $\{i, j\}$ is in imminence of colliding virtual buffers when both g_{ij}^{x} and g_{ij}^{y} are violated. Both (14) and (15) can be decomposed into two branches: an upper and a lower bound on $\mathbf{p}_i$, i.e.,

$$\begin{aligned} \mathbf{g}_{ik}^{\mathrm{u}} &= [g_{ik}^{\mathrm{xu}}\ g_{ik}^{\mathrm{yu}}]^{\intercal} \triangleq \{\mathbf{0} \leq \Delta\mathbf{p}_{ik} \leq \mathbf{d}_k\} \ , \\ \mathbf{g}_{ik}^{\mathrm{l}} &= [g_{ik}^{\mathrm{xl}}\ g_{ik}^{\mathrm{yl}}]^{\intercal} \ \triangleq \{\mathbf{0} < \Delta\mathbf{p}_{ki} \leq \mathbf{d}_k\} \ , \\ \mathbf{g}_{ij}^{\mathrm{u}} &= [g_{ij}^{\mathrm{xu}}\ g_{ij}^{\mathrm{yu}}]^{\intercal} \triangleq \{\Delta\mathbf{p}_{ij} \leq -\mathbf{r}_{ij}\} \ , \\ \mathbf{g}_{ij}^{\mathrm{l}} &= [g_{ij}^{\mathrm{xl}}\ g_{ij}^{\mathrm{yl}}]^{\intercal} \ \triangleq \{\Delta\mathbf{p}_{ji} \leq -\mathbf{r}_{ij}\} \ . \end{aligned}$$

Taking the first- and second-order time derivative of $\mathbf{g}_{ik}^{\mathrm{u}}$, $\mathbf{g}_{ik}^{\mathrm{l}}$, $\mathbf{g}_{ij}^{\mathrm{u}}$, and $\mathbf{g}_{ij}^{\mathrm{l}}$, respectively, we obtain

$$\dot{\mathbf{g}}_{ik}^{\mathrm{u}} = -\dot{\mathbf{g}}_{ik}^{\mathrm{l}} = \Delta\dot{\mathbf{p}}_{ik} \ , \quad \ddot{\mathbf{g}}_{ik}^{\mathrm{u}} = -\ddot{\mathbf{g}}_{ik}^{\mathrm{l}} = \Delta\ddot{\mathbf{p}}_{ik} \ , \tag{16}$$

$$\dot{\mathbf{g}}_{ij}^{\mathrm{u}} = -\dot{\mathbf{g}}_{ij}^{\mathrm{l}} = \Delta\dot{\mathbf{p}}_{ij} \ , \quad \ddot{\mathbf{g}}_{ij}^{\mathrm{u}} = -\ddot{\mathbf{g}}_{ij}^{\mathrm{l}} = \Delta\ddot{\mathbf{p}}_{ij} \ . \tag{17}$$

Therefore, the second-order constraint dynamics can be stabilized by Baumgarte's method as presented in II-C.

D. Regularized GPLC KKT System with Stabilization

The constrained dynamics for the swarm of swarms navigation can be expressed as (12),

$$\begin{bmatrix} \mathbf{M} & \mathbf{A}^{\intercal} \\ \mathbf{A} & -\beta\mathbf{I} \end{bmatrix} \begin{bmatrix} \ddot{\mathbf{p}} \\ \boldsymbol{\lambda} \end{bmatrix} = \begin{bmatrix} \mathbf{f} \\ \widehat{\mathbf{b}} \end{bmatrix} \ , \tag{18}$$

where $\mathbf{M} = \mathrm{diag}(\ldots, m_i, m_i, \ldots) \in \mathbb{R}^{2N \times 2N}$, $\mathbf{p} = [\ldots, \mathbf{p}_i^{\intercal}, \ldots]^{\intercal} \in \mathbb{R}^{2N}$, $\mathbf{f} = [\ldots, f_i^{\mathrm{x}}, f_i^{\mathrm{y}}, \ldots]^{\intercal} \in \mathbb{R}^{2N}$, $\forall i = 1, \ldots, N$, and each row of $\mathbf{A} \in \mathbb{R}^{C \times 2N}$ corresponds to an active constraint and has the same generic structure but different column numbers for nonzero X and Y components for $\mathbf{g}_{ik}^{\mathrm{u}}$, $\mathbf{g}_{ik}^{\mathrm{l}}$, $\mathbf{g}_{ij}^{\mathrm{u}}$, and $\mathbf{g}_{ij}^{\mathrm{l}}$, respectively. Rows of $\mathbf{A}$ for all types of constraints are presented in Table I, where we can observe that $\mathbf{A}$ contains only 1, −1, and 0. $\mathbf{A}\ddot{\mathbf{p}} = \widehat{\mathbf{b}}$ are stabilized active constraints as in (10). Note that all zero

TABLE I: ROW OF $\mathbf{A}$ FOR ALL TYPES OF CONSTRAINTS

Constraint	Row of $\mathbf{A}$	Nonzero entries' column numbers
g_{ik}^{xu} ; g_{ik}^{yu}	$[\mathbf{0}\ 1\ \mathbf{0}]$	$2i-1$; $2i$
g_{ik}^{xl} ; g_{ik}^{yl}	$[\mathbf{0}\ -1\ \mathbf{0}]$	$2i-1$; $2i$
g_{ij}^{xu} ; g_{ij}^{yu}	$[\mathbf{0}\ 1\ \mathbf{0}\ -1\ \mathbf{0}]$	$[2i-1,\ 2j-1]$; $[2i,\ 2j]$
g_{ij}^{xl} ; g_{ij}^{yl}	$[\mathbf{0}\ -1\ \mathbf{0}\ 1\ \mathbf{0}]$	$[2i-1,\ 2j-1]$; $[2i,\ 2j]$

vectors $\mathbf{0}$ in $\mathbf{A}$ as shown in the second column of Table I have the appropriate dimensions such that each row of $\mathbf{A}$ is in $\mathbb{R}^{2N}$.

E. Deadlock Resolution

In the presented MAMS navigation problem, deadlocks occurs in which one or more agent is blocked from progressing towards its virtual leader under nonzero control actions for leader following. Specifically, when the actions of leader following constraints are colinear with the actions of collision avoidance constraints, the leader following control actions attempt to pull the colliding agents through each other, resulting in potential deadlocks.

The normal component of $\Delta\dot{\mathbf{p}}_{ij}$ between colliding agents $\{i,j\}$, $\frac{d}{dt}\|\Delta\mathbf{p}_{ij}\| = \frac{\Delta\mathbf{p}_{ij}^{\mathsf{T}}}{\|\Delta\mathbf{p}_{ij}\|}\Delta\dot{\mathbf{p}}_{ij}$, contributes to collision, while the tangential component of $\Delta\dot{\mathbf{p}}_{ij}$ leads to only rotation about each other. $\|\cdot\|$ denotes 2-norm of a vector. Hence, the most dangerous scenario is $\{i,j\}$ undergoing a head-on collision when $\frac{d}{dt}\|\Delta\mathbf{p}_{ij}\| = \|\Delta\dot{\mathbf{p}}_{ij}\|$.

In our earlier work [11], the leader following and collision avoidance of a single navigating swarm are described as scalar constraints in terms of $\|\Delta\mathbf{p}_{ik}\|^2$ ($k \equiv 1$ since there is only one virtual leader) and $\|\Delta\mathbf{p}_{ij}\|^2$, respectively. Hence, the symbolic entries of the corresponding $\mathbf{A}$ ($\Delta\mathbf{p}_{ik}^{\mathrm{x}}$ and $\Delta\mathbf{p}_{ik}^{\mathrm{y}}$, and, $\Delta\mathbf{p}_{ji}^{\mathrm{x}}$, $\Delta\mathbf{p}_{ji}^{\mathrm{y}}$, $\Delta\mathbf{p}_{ij}^{\mathrm{x}}$, and $\Delta\mathbf{p}_{ij}^{\mathrm{y}}$. Computed as (4), see Equation (25) in [11] for more details.) are the respective functions of $\Delta\mathbf{p}_{ik}$ and $\Delta\mathbf{p}_{ij}$ and, thus, the corresponding control forces $-\mathbf{A}^{\mathsf{T}}\boldsymbol{\lambda}$ align with $\Delta\mathbf{p}_{ik}$ and $\Delta\mathbf{p}_{ij}$, respectively. Therefore, a deadlock for agent i occurs when scalar leader following (between agent i and the virtual leader) and collision avoidance (between agent i and j) constraints are both active and when $\Delta\mathbf{p}_{ik}$, $\Delta\dot{\mathbf{p}}_{ik}$, $\Delta\mathbf{p}_{ij}$, and $\Delta\dot{\mathbf{p}}_{ij}$ are colinear.

In this work, decomposed constraints $\mathbf{g}_{ik}$ and $\mathbf{g}_{ij}$ provide independent control forces along the X and Y axes, allowing naturally for a multi-swarm formulation and deadlock resolution. By having different control parameters ζ, ω, $\mathbf{d}_k$, and $\mathbf{r}_{ij}$ for $\ddot{\mathbf{g}}_{ik}$ and $\ddot{\mathbf{g}}_{ij}$ stabilization, the proposed decomposed constraint formulation can provide more maneuverability in a collision and thus deadlock than that of the scalar constraint formulation in [11], in which the control forces for colinear active leader following and collision avoidance constraints on one agent are always in opposite directions.

Selecting the branch (upper or lower) to take the value zero for active decomposed collision constraints g_{ij}^{x} and g_{ij}^{y} completes the deadlock resolution scheme. Note that in the GPLC control, the Lagrange multipliers associated with active constraints are nonzero for all time. In [11], when the virtual buffers of an agent pair $\{i,j\}$ are about to collide under either $|\Delta\mathbf{p}_{ij}^{\mathrm{x}}|$ (i.e., g_{ij}^{x}) or $|\Delta\mathbf{p}_{ij}^{\mathrm{y}}|$ (i.e., g_{ij}^{y}) being exactly zero, the corresponding symbolic entries in $\mathbf{A}$ ($\Delta\mathbf{p}_{ij}^{\mathrm{x}}$ and $\Delta\mathbf{p}_{ji}^{\mathrm{x}}$, or, $\Delta\mathbf{p}_{ij}^{\mathrm{y}}$ and $\Delta\mathbf{p}_{ji}^{\mathrm{y}}$) and thus the corresponding command control in $-\mathbf{A}^{\mathsf{T}}\boldsymbol{\lambda}$ will also be zero, i.e., no control action to avoid crash along that axis for the colliding agent pair $\{i,j\}$, leading to potential deadlocks. In this work, the nonzero entries in $\mathbf{A}$ corresponding to g_{ij}^{x} and g_{ij}^{y} are either 1 or -1 regardless of the values of $\Delta\mathbf{p}_{ij}^{\mathrm{x}}$ and $\Delta\mathbf{p}_{ij}^{\mathrm{y}}$. Hence, the command controls for agent i and j corresponding to collision avoidance along the X and Y axes have nonzero identical magnitudes but opposite direction, respectively.

In this study, a subset of decomposed collision constraints are selected to include equality to zero such that the active $\mathbf{g}_{ij}^{\mathrm{u}}$ and $\mathbf{g}_{ij}^{\mathrm{l}}$ are respectively $\{-\mathbf{r}_{ij} < \Delta\mathbf{p}_{ij} \leq \mathbf{0}\}$ and $\{\mathbf{0} < \Delta\mathbf{p}_{ij} < \mathbf{r}_{ij}\}$. Therefore, $\forall\Delta\mathbf{p}_{ij} \in (-\mathbf{r}_{ij},\ \mathbf{r}_{ij})$, the control actions for collision avoidance are nonzero and can achieve any direction in a 2-D plane by adjusting ζ, ω, and $\mathbf{r}_{ij}$.

F. Actuator Saturation and Dynamics

We assume as in [11] that the actuator is subjected to saturation $\mathbf{f}_{\mathrm{c}} = \min\{\max\{-\mathbf{A}^{\mathsf{T}}\boldsymbol{\lambda},\ \mathbf{f}_{\mathrm{l}}\},\ \mathbf{f}_{\mathrm{u}}\}$ and the first-order dynamics $\dot{\mathbf{f}}_{\mathrm{a}} = (\mathbf{f}_{\mathrm{c}} - \mathbf{f}_{\mathrm{a}})/\tau$, where $\mathbf{f}_{\mathrm{l}}$ and $\mathbf{f}_{\mathrm{u}}$ are respectively the lower and upper bound for command control force, $\mathbf{f}_{\mathrm{c}}$ is the saturated command control force, $\mathbf{f}_{\mathrm{a}}$ is the actual control force, and 0.05 sec $\lessapprox \tau \lessapprox 1.0$ sec is a time constant. Note that $\dot{\mathbf{f}}_{\mathrm{a}}$ is bounded automatically given that $\mathbf{f}_{\mathrm{a}} = \mathbf{0}$ at $t = 0$.

With the saturated and delayed actuator force $\mathbf{f}_{\mathrm{a}}$, the actual acceleration is updated as $\hat{\ddot{\mathbf{p}}} = \mathbf{M}^{-1}(\mathbf{f} + \mathbf{f}_{\mathrm{a}})$. The vector of state derivatives $[\dot{\mathbf{p}}^{\mathsf{T}}\ \hat{\ddot{\mathbf{p}}}^{\mathsf{T}}\ \dot{\mathbf{f}}_{\mathrm{a}}^{\mathsf{T}}]^{\mathsf{T}}$ is then used in the numerical integration.

IV. NUMERICAL RESULTS

The proposed method is numerically implemented in MATLAB on a Windows laptop with a 2.50 GHz Intel i5-7200U CPU and 8 GB memory. Noting that our framework can readily cope with heterogeneous agents, we adopt homogeneous agents in this work. The parameters used in this study are: $m_i = 10$ kg, $g = 9.8$ kg/m^2, $\omega_{ik}^{\mathrm{x}} = \omega_{ik}^{\mathrm{y}} = 3$ rad/s, $\omega_{ij}^{\mathrm{x}} = \omega_{ij}^{\mathrm{y}} = 4$ rad/s, $\zeta_{ik}^{\mathrm{x}} = \zeta_{ik}^{\mathrm{y}} = 1$, $\zeta_{ij}^{\mathrm{x}} = \zeta_{ij}^{\mathrm{y}} = 1$, $\beta = m_i/10^4$, $\tau = 0.1$ s, and $\mathbf{f}_{\mathrm{u}} = -\mathbf{f}_{\mathrm{l}} = 5m_i g\,\mathbf{1}$ N, where $\mathbf{1}$ is a length-$2N$ vector full of ones. The time integrator used is the fourth-order Runge-Kutta method with a constant time step of 0.005 s. The virtual leaders start and end at positions symmetric about the Y axis with zero velocities and remain stationary at the end positions for 5 s. The motions of the leaders have the same magnitude but opposite sign. All agents start from zero initial velocities, and the exogenous forces are assumed to be zero for all time, as the external disturbances can break the symmetry in a deadlock and thus making the deadlock resolution less challenging.

A. Head-on Collision of Two Agents

Fig. 1 shows the trajectories of agents 1 and 2 exchanging their regions by following two virtual leaders that swap their initial and goal positions at $[10,\ 0]$ and $[-10,\ 0]$. The

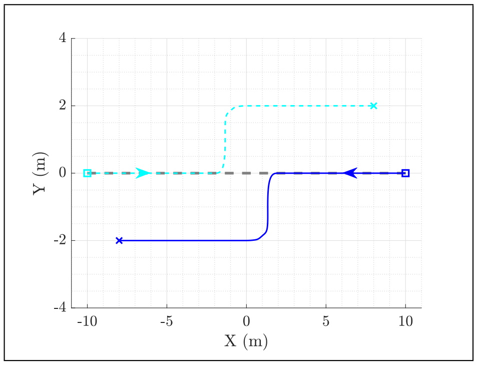

Fig. 1: Trajectories of two virtual leaders and two agents. The gray dashed lines are the paths of two virtual leaders. The solid lines are the agents' path, with □ and × respectively denoting start and end positions. The agents come to a deadlock midway but resolve it by reacting purely to the constrained dynamics. The corresponding animation can be found online. [1]

parameters $\mathbf{d}_k$ and $\mathbf{r}_{ij}$ used in this case study are $d_k^{\mathrm{x}} = d_k^{\mathrm{y}} = 2$ m and $r_{ij}^{\mathrm{x}} = r_{ij}^{\mathrm{y}} = 4$ m. This is a perfectly symmetric problem. The agents run into a head-on collision at $x_1 = 2$ m and $x_2 = -2$ m with the active g_{ij}^{y} being exactly zero, leading to a deadlock.

After solving (18), the command control actions for avoiding collision between the two agents are the multiplication of 1 and -1 in the row of $\mathbf{A}$ with $\lambda_{12}^{\mathrm{c}}$ that corresponds to active $\mathbf{g}_{12}$. Hence, the collision avoidance control actions of the two agents have the same magnitude but opposite sign in both X and Y axes.

From Fig. 2, we can observe that the agents satisfy the following and collision constraints and thus have no control actions for $t \in [0, 2.5)$ s. The onset of control forces at $t = 2.5$ s corresponds to both agents violating $\mathbf{g}_{ik}^{\mathrm{x}}$ for the first time. Then, the control forces asymptotically converge to zero due to the enforced Baumgarte's stabilization on active constraint dynamics. The agents are in danger of colliding virtual buffers at $t = 5$ s, when a collision avoidance constraint first becomes active. Since both $\mathbf{g}_{ik}$ and $\mathbf{g}_{ij}$ are critically damped, $\omega_{ik} < \omega_{ij}$, in a deadlock the control actions for collision constraints prevail over those for leader following. For $t \in [5, 8]$ s, the agents are subjected to active collision constraints in both axes and active following constraint in X axis, and the combined control actions due to two active types of constraints repel the agents away from each other. Finally, for $t \in [8, 15]$ s, the collision constraints become inactive, and the agents are driven towards their leaders due to active following constraints along the X and Y directions. Since the second-order dynamics for both types of constraints are critically damped, the relative distances along the X and Y axes are asymptotically stabilized to the thresholds d_k^{x} and d_k^{y} for $t \in [10, 15]$ s.

B. Head-on Collision of Two Swarms

Fig. 3 presents the trajectories of two 15-agent swarms guided by two virtual leaders flipping positions between $[30, 0]$ and $[-30, 0]$. $\mathbf{d}_k$ and $\mathbf{r}_{ij}$ in this case study are $d_k^{\mathrm{x}} = d_k^{\mathrm{y}} = d = 9$ m and $r_{ij}^{\mathrm{x}} = r_{ij}^{\mathrm{y}} = r = 4$ m. The

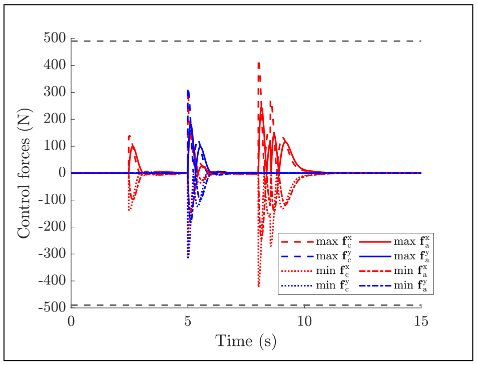

Fig. 2: The maximum and minimum command and actual control forces, $\mathbf{f}_{\mathrm{c}}$ and $\mathbf{f}_{\mathrm{a}}$. The gray dashed lines denote the actuator saturation bounds. $\mathbf{f}_{\mathrm{c}}$ precedes $\mathbf{f}_{\mathrm{a}}$ due to first-order actuator dynamics. The controls are asymptotically stabilized to zero due to constraint dynamics (9).

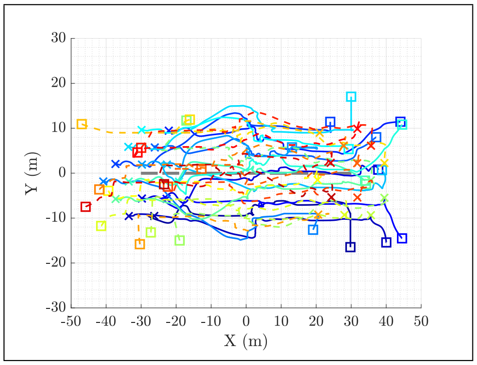

Fig. 3: Navigation trajectories of 2 swarms of 15 agents. The solid lines and the dashed lines are respectively the agents' paths for swarm 1 and 2. □ and × respectively denote the initial and goal positions for both swarms. The agents come to a deadlock about midway but resolve it by reacting purely to the constrained two-swarm dynamics. The corresponding animation is available online. [2]

X and Y initial positions of all agents are generated from two sequences of uniformly distributed random numbers within the intervals $(-2d_k^{\mathrm{x}}, 2d_k^{\mathrm{x}})$ and $(-2d_k^{\mathrm{y}}, 2d_k^{\mathrm{y}})$ around the leaders' initial positions, respectively. Note that this random initialization does not obey all constraints and thus the system is in the controlled space from $t = 0$.

From Figs. 4 and 5, we observe that the randomly generated initial positions do not satisfy all collision and following constraints; however, the bounds on the constraint errors and thus the individual constraint error asymptotically converge to zero during the swarm navigation for $t \in [2, 8]$ s, where the bounds on control forces are smaller than the initial stage in which the constraint errors are larger. In the middle of the leaders' motions, multiple agent pairs run into potential deadlocks. Since the head-on collision of the two swarms occurs along the X axis, the constraint errors for both types of constraints are in general larger in the X axis than those in the Y axis. The agents violate the following constraints and resolve collision deadlock by reacting purely to the constrained two-swarm dynamics, and the constraint errors are asymptotically driven to admissibility. For $t \in [18, 20]$ s, the constraints are slightly violated, as evidenced by the

[1] https://youtu.be/ogNqEoryYIQ

[2] https://youtu.be/10CXrmDop48

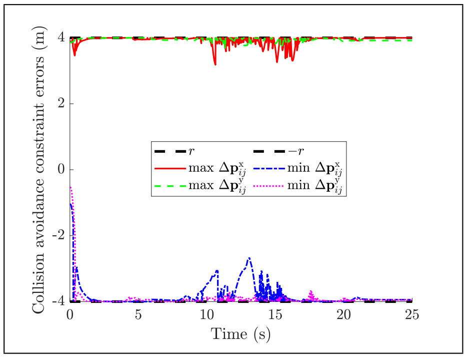

Fig. 4: The maximum and minimum active collision avoidance constraint errors.

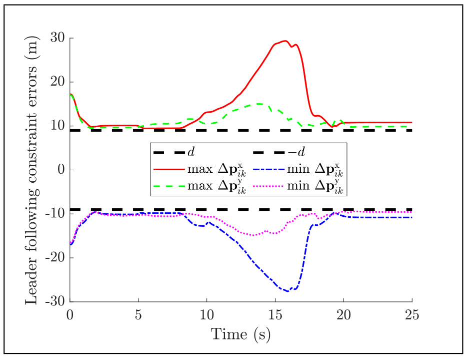

Fig. 5: The maximum and minimum leader following constraint errors.

overall decreasing control forces in Fig. 6. Finally, when the leaders remain stationary for $t \in [20, 25]$ s, the constraint errors remain constant over time, and the control forces smoothly converge to zero, indicating that all agents come to a stop.

The elapsed real time for control actions calculation considers the time accumulated over the simulation span to identify active constraints, to construct and solve (18), and to compute and saturate the control actions $\mathbf{f}_c$. Then, the computation time per time step is obtained by dividing the total accumulative elapsed time by the total number of integration steps. In this case study, the computation time per time step is 2.5374×10^{-5} s, indicating the efficiency of the proposed approach.

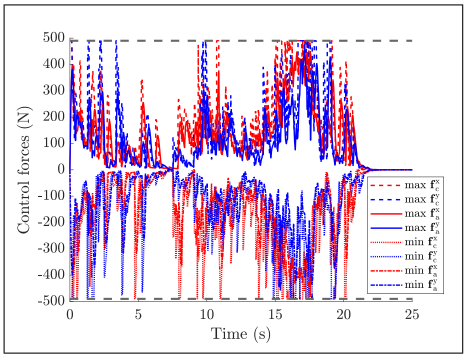

Fig. 6: The maximum and minimum command and actual control forces, $\mathbf{f}_c$ and $\mathbf{f}_a$, for 2-swarm head-on collision. Both leaders are static at the goal positions for $t \in [20, 25]$ s. The gray dashed lines denote the actuator saturation bounds. $\mathbf{f}_c$ precedes $\mathbf{f}_a$ due to first-order actuator dynamics.

V. Conclusions and Future Work

This paper extends the application of Gauss's Principle of Least Constraint to the navigation of MAMS systems to meet leader following and collision avoidance objectives. By decomposing inequality constraints for leader following and collision avoidance into separate constraints for each coordinate and by asymmetrically allowing constraints to be satisfied with an equality to zero, or restricting the constraint to a strict inequality, the method provides a heuristic-free and computationally efficient nonlinear feedback control law for the navigation of agents to follow leaders and to negotiate potential collisions and potential deadlocks.

To further this line of research, the proposed method can be enhanced by examining its scalability for the computational efficiency and its performance under parametric uncertainties, modeling errors, and obstacle avoidance. Moreover, the decentralized and distributed counterparts of the proposed control scheme would be an interesting topic of future work.

References

[1] Y. Liu and R. Bucknall, "A survey of formation control and motion planning of multiple unmanned vehicles," *Robotica*, vol. 36, no. 7, pp. 1019–1047, 2018.

[2] S. Huang, R. S. H. Teo, and K. K. Tan, "Collision avoidance of multi unmanned aerial vehicles: A review," *Annu. Rev. Contr.*, vol. 48, pp. 147–164, 2019.

[3] J. Van Den Berg, S. J. Guy, M. Lin, and D. Manocha, "Reciprocal n-body collision avoidance," in *Int. Symp. Robot. Res.*, 2011, pp. 3–19.

[4] J. A. Douthwaite, S. Zhao, and L. S. Mihaylova, "Velocity obstacle approaches for multi-agent collision avoidance," *Unmanned Syst.*, vol. 7, no. 01, pp. 55–64, 2019.

[5] N. E. Leonard and E. Fiorelli, "Virtual leaders, artificial potentials and coordinated control of groups," in *Proc. IEEE Conf. Decis. Control*, vol. 3. IEEE, 2001, pp. 2968–2973.

[6] M. T. Wolf and J. W. Burdick, "Artificial potential functions for highway driving with collision avoidance," in *Proc. IEEE Int. Conf. Robot. Autom.*, 2008, pp. 3731–3736.

[7] T. Schouwenaars, B. De Moor, E. Feron, and J. How, "Mixed integer programming for multi-vehicle path planning," in *Euro. Control Conf.*, 2001, pp. 2603–2608.

[8] D. Mellinger, A. Kushleyev, and V. Kumar, "Mixed-integer quadratic program trajectory generation for heterogeneous quadrotor teams," in *Proc. IEEE Int. Conf. Robot. Autom.*, 2012, pp. 477–483.

[9] L. Wang, A. D. Ames, and M. Egerstedt, "Safety barrier certificates for collisions-free multirobot systems," *IEEE Trans. Robot.*, vol. 33, no. 3, pp. 661–674, 2017.

[10] J. Grover, C. Liu, and K. Sycara, "Deadlock analysis and resolution in multi-robot systems (extended version)," *arXiv preprint arXiv:1911.09146*, 2019.

[11] B. Zhang and H. P. Gavin, "Gauss's principle with inequality constraints for multi-agent navigation and control," *IEEE Trans. Automat. Contr.*, 2021. [Online]. Available: http://dx.doi.org/10.1109/TAC.2021.3059677

[12] F. E. Udwadia and R. E. Kalaba, "A new perspective on constrained motion," *Proc.: Math. Phys. Sci.*, vol. 439, no. 1906, pp. 407–410, 1992.

[13] B. Shirani, M. Najafi, and I. Izadi, "Cooperative load transportation using multiple UAVs," *Aerosp. Sci. Technol.*, vol. 84, pp. 158–169, 2019.

[14] R. Zhao, M. Li, Q. Niu, and Y.-H. Chen, "Udwadia-Kalaba constraint-based tracking control for artificial swarm mechanical systems: dynamic approach," *Nonlinear Dyn.*, 2020.

[15] J. Baumgarte, "Stabilization of constraints and integrals of motion in dynamical systems," *Comput. Methods in Appl. Mech. Eng.*, vol. 1, no. 1, pp. 1–16, 1972.